

SLAC - PUB - 4066

COLO - HEP - 132

April 1987

E

**Measurement of the polarization of  $\tau$  leptons  
produced in  $e^+e^-$  annihilation at  $\sqrt{s} = 29 \text{ GeV}^*$**

W. T. Ford, N. Qi, A. L. Read, Jr.,<sup>(a)</sup> and J. G. Smith  
*Department of Physics, University of Colorado, Boulder, Colorado 80309*

T. Camporesi,<sup>(b)</sup> R. De Sangro, I. Peruzzi, and M. Piccolo  
*I. N. F. N., Laboratori Nazionali di Frascati, Frascati, Italy*

R. B. Hurst, J. Pyrlík, J. P. Venuti, and R. Weinstein  
*Department of Physics, University of Houston, Houston, Texas 77004*

M. W. Gettner, G. P. Goderre,<sup>(c)</sup> J. C. Sleeman, and E. von Goeler  
*Department of Physics, Northeastern University, Boston, Massachusetts 02115*

G. B. Chadwick, R. E. Leedy, R. L. Messner, L. J. Moss, F. Müller,<sup>(d)</sup>  
H. N. Nelson, D. M. Ritson, L. J. Rosenberg,<sup>(e)</sup> D. E. Wiser, and R. W. Zdarko  
*Department of Physics and Stanford Linear Accelerator Center,  
Stanford University, Stanford, California 94305*

D. E. Groom and P. G. Verdini  
*Department of Physics, University of Utah, Salt Lake City, Utah 84112*

H. R. Band, M. C. Delfino,<sup>(f)</sup> J. R. Johnson, T. L. Lavine, T. Maruyama, and R. Prepost  
*Department of Physics, University of Wisconsin, Madison, Wisconsin 53706*

Submitted to *Physical Review D*

---

\* This work was supported in part by the Department of Energy under contract numbers DE-AC02-81ER40025 (CU), DE-AC03-76SF00515 (SLAC), and DE-AC02-76ER00881 (UW); by the National Science Foundation under grant numbers NSF-PHY82-15133 (UH), NSF-PHY82-15413 and NSF-PHY82-15414 (NU), and NSF-PHY83-08135 (UU); and by the Istituto Nazionale di Fisica Nucleare.

## ABSTRACT

We present measurements of forward-backward energy asymmetries of tau lepton decay products from the reaction  $e^+e^- \rightarrow \tau^+\tau^-$  in data collected with the MAC detector operating at the SLAC storage ring PEP at a center-of-mass energy of 29 GeV. The energy asymmetries for the decays  $\tau \rightarrow \nu_\tau e \bar{\nu}_e$ ,  $\tau \rightarrow \nu_\tau \mu \bar{\nu}_\mu$ ,  $\tau \rightarrow \nu_\tau \pi$ , and  $\tau \rightarrow \nu_\tau \rho$  are interpreted as effects caused by the combination of maximally parity-violating weak tau decays and a longitudinal polarization produced by the interference of electromagnetic and weak processes. From the forward-backward polarization asymmetry  $A_P = (0.06 \pm 0.07) \times (1 \pm 0.011)$ , we determine the tau coupling constant product  $g_a^e g_v^\tau = (0.26 \pm 0.31) \times (1 \pm 0.011)$ . Assuming  $g_a^e = -1/2$  as expected, we find  $g_v^\tau = (-0.52 \pm 0.62) \times (1 \pm 0.011)$ , consistent with the prediction of the Glashow-Weinberg-Salam model of electroweak interactions. Alternatively, assuming the standard model prediction of negligible polarization in tau-pair production, the leptonic energy spectra are used to measure the Michel parameter to be  $0.79 \pm 0.10 \pm 0.10$ , consistent with the  $V - A$  hypothesis for the  $\tau \bar{\nu}_\tau W$  vertex.

## I. INTRODUCTION

A crucial test of the Glashow-Weinberg-Salam (GWS) model<sup>1</sup> of electroweak interactions is to verify that the interaction of the weak neutral current with the  $\tau$  lepton is correctly described. In this model the coupling constants of leptons ( $l$ ) to the axial vector and vector components of the weak neutral current are given by  $g_a^l = -1/2$  and  $g_v^l = -1/2 + 2 \sin^2 \theta_W$ , respectively. Values for the coupling constant products  $g_a^e g_a^\tau$  and  $g_v^e g_v^\tau$  have been obtained from measurements of the forward-backward asymmetry in the differential cross section and the total cross section for  $e^+e^- \rightarrow \tau^+\tau^-$ , respectively. These measurements are consistent with the predictions of the GWS model; however, since  $g_v^l$  is quite small (the current world average of  $\sin^2 \theta_W = 0.22^2$  implies that  $g_v^l = -0.06$ ), the experimental error in  $g_v^\tau$  is typically  $\sim \pm 2$  or larger. The mean tau polarization and forward-backward polarization asymmetry are proportional to  $g_v^e g_a^\tau$  and  $g_a^e g_v^\tau$ , respectively. These coupling constant products are expected to be an order of magnitude larger than  $g_v^e g_v^\tau$ , allowing a more precise determination of  $g_v^\tau$ .

In this paper, we report measurements of forward-backward energy asymmetries and mean energies of the tau lepton decay products  $e, \mu, \pi$ , and  $\rho$  with taus produced in the reaction  $e^+e^- \rightarrow \tau^+\tau^-$ . From these measurements, the polarization and polarization asymmetry of the taus are extracted, yielding values for the tau weak neutral current couplings if a standard  $V - A$  tau decay mechanism is assumed. Also presented is an analysis of the energy spectra of the leptonic decays, assuming negligible tau polarization as expected from the GWS model, which yields a measurement of the Michel parameter  $\rho$  and provides a test of the  $V - A$  decay interaction. The data were collected with the MAC de-

tector operating at the Stanford Linear Accelerator Center storage ring PEP at a center-of-mass energy of 29 GeV. The parent data sample consists of more than 10000 identified tau decays representing an integrated luminosity of  $212.7 \pm 3.3$  pb<sup>-1</sup>.

The spin dependent cross section for the process  $e^+e^- \rightarrow \tau^+\tau^-$  with unpolarized beams, calculated from the Feynman diagrams in Fig. 1 and including only terms of order  $\alpha^2$  and  $\alpha G_F$ , is<sup>3</sup>

$$\frac{d\sigma(\vec{s}_-, \vec{s}_+)}{d\Omega} = \frac{\alpha^2 \beta}{4s} [(1 - rg_v^e g_v^T) t_1 + rg_a^e g_a^T t_2 + rg_a^e g_v^T t_3 - rg_v^e g_a^T t_4] \quad (1)$$

where

$$\begin{aligned} r &= \frac{G_F}{\pi\sqrt{2}\alpha} \frac{sM_Z^2}{M_Z^2 - s}, \\ t_1 &= 1 + \cos^2\theta + \frac{1}{\gamma^2} \sin^2\theta + s_z^+ s_z^- (1 + \cos^2\theta - \frac{1}{\gamma^2} \sin^2\theta) \\ &\quad + s_x^- s_x^+ \frac{1}{\gamma^2} \sin^2\theta - s_y^- s_y^+ \beta^2 \sin^2\theta - (s_x^- s_z^+ + s_z^- s_x^+) \frac{1}{\gamma} \sin 2\theta, \\ t_2 &= -2\beta \cos\theta (1 + s_z^- s_z^+) + (s_x^- s_z^+ + s_z^- s_x^+) \frac{\beta}{\gamma} \sin\theta, \\ t_3 &= 2(s_z^- + s_z^+) \cos\theta - 2(s_x^- + s_x^+) \frac{1}{\gamma} \sin\theta, \text{ and} \\ t_4 &= -(s_z^- + s_z^+) \beta (1 + \cos^2\theta) + (s_x^- + s_x^+) \frac{\beta}{2\gamma} \sin 2\theta. \end{aligned} \quad (2)$$

The polar angle between the outgoing  $\tau^-$  and the incoming  $e^-$  is  $\theta$ ,  $s$  is the center-of-mass energy squared,  $M_Z$  is the mass of the weak neutral boson,  $\beta$  is the velocity of the taus in the laboratory in units of the velocity of light,  $\gamma$  is  $1/\sqrt{1 - \beta^2}$ , and  $\alpha$  is the electromagnetic coupling constant,  $e^2/4\pi$ . The tau spins  $\vec{s}_\pm$  are calculated in their respective centers of mass using a coordinate system

for which the z-axis points along the direction of flight of the  $\tau^-$ , the x-axis is formed from the cross product of the  $e^-$  direction with the z-axis, and the y-axis completes a right handed coordinate system. Since  $\sqrt{s}$  is small compared with  $M_Z$ , the Z width has been neglected in  $r$ .

The longitudinal polarization of the  $\tau^-$ , defined by

$$P_\tau = \frac{d\sigma(s_z^- = +1) - d\sigma(s_z^- = -1)}{d\sigma(s_z^- = +1) + d\sigma(s_z^- = -1)}, \quad (3)$$

can be calculated from Eq. (1):

$$P_\tau = r \frac{g_v^e g_a^\tau \beta (1 + \cos^2 \theta) + g_a^e g_v^\tau 2 \cos \theta}{(1 + \cos^2 \theta + \frac{1}{\gamma^2} \sin^2 \theta)(1 - r g_v^e g_v^\tau) - r g_a^e g_a^\tau 2 \beta \cos \theta}. \quad (4)$$

With  $\sqrt{s} = 29$  GeV,  $r$  and  $g_v$  are expected to be sufficiently small that  $P_\tau$  can be approximated by

$$P_\tau = r (g_v^e g_a^\tau + \frac{2 \cos \theta}{1 + \cos^2 \theta} g_a^e g_v^\tau). \quad (5)$$

A measurement of the polarization averaged over solid angle, given by

$$\langle P \rangle = r g_v^e g_a^\tau, \quad (6)$$

is sensitive only to  $g_v^e g_a^\tau$  whereas a measurement of the polarization asymmetry, given by

$$A_P \equiv \frac{1}{2} (P_F - P_B) = r g_a^e g_v^\tau \frac{3x^2}{3x + x^3}, \quad (7)$$

is sensitive only to  $g_a^e g_v^\tau$ .  $P_F$  and  $P_B$  are the average polarizations for  $\cos \theta > 0$  and  $\cos \theta < 0$ , respectively, and  $x$  is the maximum observable  $|\cos \theta|$ . The average

polarization is expected to be 1.01% and the polarization asymmetry to be 0.76% (0.72%) for  $|\cos \theta| < 1.0$  (0.9) at  $\sqrt{s} = 29$  GeV for the world average values  $\sin^2 \theta_W = 0.22$  and  $M_Z = 93$  GeV/c<sup>2</sup>.<sup>4</sup>

The polarization can be measured from the angular distribution, with respect to the polarization axis, of the tau decay products in the tau center-of-mass system. However, in the laboratory frame, this angular distribution is observed as an angle and energy distribution due to the Lorentz boost. Since unobserved neutrinos make it impossible to reconstruct the original tau direction in leptonic decays and experimentally difficult in semi-leptonic decays, it is most practical simply to observe single particle energy spectra and ignore the angular correlation of the decay products of the two taus.

## II. APPARATUS

The MAC detector<sup>5</sup> consists of a cylindrical drift chamber inside a conventional solenoid coil, surrounded by a hexagonal array of electromagnetic and hadronic calorimeters, scintillation counters, and drift chambers for detection of muons. End caps on either side of the central detector complete the coverage to within about 10° of the beams.

The central drift chamber (CD) consists of 833 double sense wire cells arranged in 10 layers coaxial with the beams. The 180  $\mu\text{m}$  resolution of the CD results in typical angular resolutions of 0.2° in azimuth ( $\phi$ ) and 0.7° in polar angle and, together with the 0.57 T axial magnetic of the solenoid coil, field results in an inverse momentum resolution of about  $\sigma_{1/p} = 0.052 \sin \theta$  (GeV/c)<sup>-1</sup>. Particles

originating from the interaction point traverse at least nine layers of the CD for polar angles such that  $|\cos \theta| < 0.9$ .

The central section electromagnetic and hadronic calorimeters are constructed of alternating layers of proportional wire chambers (PWC's) and 0.25-cm thick lead sheets and 2.5-cm thick iron plates, respectively. The end caps consist entirely of alternating layers of PWC's and 2.5-cm thick iron plates. The energy resolutions for electromagnetic showers are  $\sigma_E/E = 20\%/\sqrt{E(\text{GeV})}$  in the central section and  $45\%/\sqrt{E}$  in the end caps. For hadronic showers the hadronic calorimeters have energy resolutions of about  $75\%/\sqrt{E}$ . The electromagnetic calorimeters have angular resolutions of  $\sigma_\phi = 0.6^\circ$  and  $\sigma_\theta = 1.2^\circ$  in the central section and  $\sigma_\phi = 1.2^\circ$  and  $\sigma_\theta = 1.5^\circ$  in the end caps. The central section PWC's are constructed of wires strung parallel to the beams and the  $z$ -position of charge deposition on a wire is measured with current division techniques. The end cap PWC's are constructed of azimuthally segmented aluminium cathode strips and anode wire groups with segmentation in polar angle. Measurement of both  $\phi$  and  $\theta$  is accomplished by readout of both anodes and cathodes.

The outer drift system (OD) is used to identify muons and measure their momenta. The entire system consists of 2416 drift chamber cells. The calorimeters are surrounded by a hexagonal barrel of four layers of cylindrical drift tubes oriented transverse to the beams, except for the plane under the detector which consists of three layers of planar drift chambers. The ends of the detector are covered with six planes of drift tubes, covering the angular range  $0.80 < |\cos \theta| < 0.97$ . The iron calorimeters are magnetized with a toroidal field strength of 1.75 T and the OD measures the polar bend angle of a charged particle emerging from the

iron. The average inverse momentum resolution is  $\sigma_{1/p}/(1/p) = 0.30$ , dominated by multiple scattering.

The time-of-flight (TOF) system covers 97% of the solid angle with 144 plastic scintillation counters read out by photomultiplier tubes. The 72 central section counters form a hexagonal barrel enclosing the central section electromagnetic calorimeter. The remaining 72 counters provide particle detection at low angles and are placed, 36 in each end cap, after the sixth iron plate of the end cap calorimeter (near the region in which electromagnetic showers deposit most of their energy). With typical distances from the interaction point of 2-4 meters, cosmic ray induced TOF hits on opposite sides of the detector have a time difference of about 10 nsec, while hits produced by tracks from  $e^+e^-$  annihilation occur at roughly the same time. The TOF resolution is about 1 nsec.

The trigger for the experiment consists of the logical OR of (1) scintillator hits in opposite sextants or end cap quadrants; (2) scintillator hits on three or more of the eight faces of the detector (six sextant faces and two end cap planes); (3) showers of at least 2 GeV in any two of six shower chamber sextants, two end caps, or the central hadron calorimeter; (4) one or more penetrating tracks, defined by a cluster of CD hits in azimuthal coincidence with energy deposition of more than 400 MeV in the matching calorimeter sextant and a signal in one of the corresponding scintillators. Events satisfying this hardware trigger must also pass a simple software filter. The data were logged onto magnetic tapes and then subjected to a loose first-pass analysis that rejected 90% of the original triggers and left about  $4 \times 10^6$  events (mostly from Bhabha scattering) for subsequent analysis.

### III. TAU DECAY SAMPLE

#### A. Event selection

The tau data sample is selected from the low-multiplicity events by specific discrimination against the possible backgrounds. All two- and four-prong final states are included except those two-prongs in which both are electrons or both muons, which cannot be adequately separated from backgrounds of the processes

$$e^+e^- \rightarrow e^+e^-(\gamma), \quad (8)$$

$$e^+e^- \rightarrow \mu^+\mu^-(\gamma), \quad (9)$$

$$e^+e^- \rightarrow (e^+e^-)e^+e^-, \quad (10)$$

$$e^+e^- \rightarrow (e^+e^-)\mu^+\mu^-, \quad (11)$$

and cosmic rays. The cross sections of two-photon processes (10) and (11) are largest when the initial state electron and positron scatter at low angles and do not appear in the detector. The rejected  $ee$  and  $\mu\mu$  final states constitute only 6% of all produced tau-pairs. Final states in which both taus decay into 3 or 5 charged particles (2% of produced tau-pairs) have large backgrounds from the reactions

$$e^+e^- \rightarrow q\bar{q}(\gamma), \text{ and} \quad (12)$$

$$e^+e^- \rightarrow (e^+e^-)q\bar{q}. \quad (13)$$

Background from the process

$$e^+e^- \rightarrow (e^+e^-)\tau^+\tau^- \quad (14)$$

is also of concern since it closely resembles the signal. The selection criteria

were developed with studies of their effect on a Monte Carlo sample with full detector simulation. The reliability of the simulation was checked by comparison of appropriate distributions with the data (see below).

Events are required to have either two or four tracks reconstructed in the CD; at least two of these are required to have a satisfactory  $\chi^2$  for a constrained fit to a vertex originating at the interaction point (primary vertex). Tracks in reconstructed  $e^+e^-$  photon conversion pairs are not counted as prongs. Events with two prongs are rejected if both are identified as electrons or muons because of the large backgrounds from reactions (8)-(11) as discussed above. Background from processes (12) and (13) is reduced by requiring that one charged track be separated from all others by at least  $120^\circ$ , the charged particle sphericity be less than 0.05, and the net transverse momentum relative to the thrust axis be less than 1.5 GeV/c. The latter two requirements also reduce background from events produced in beam-gas interactions. Requiring the electromagnetic shower energy to be less than 23 GeV effectively rejects most Bhabba scattering events. To obtain further rejection of process (8) as well as of processes (10) and (11), events containing an identified electron with an energy greater than 5 GeV and a small angle to the beam axis are removed, as are those with tracks passing near inactive regions of the calorimeters or a single large spurious hit in the hadron calorimeters. Track quality cuts are made primarily to reduce background from very low angle events from Bhabba scattering. Radiative events from processes (8) and (9) are reduced by eliminating events with neutrals which are consistent with a kinematic fit to an  $ee\gamma$  or  $\mu\mu\gamma$  hypothesis. Background from all two-photon collision processes is reduced by requiring the total calorimetric energy

to be greater than 6 GeV and the scalar sum of the CD momenta to be greater than 2 GeV/c. To reject QED backgrounds (especially process (8)) and cosmic ray events, events with two tracks are required to be acollinear by more than  $1^\circ$  and acoplanar (the deviation from collinearity in the plane transverse to the beam axis) by more than  $1^\circ$  and less than  $40^\circ$ . For a further reduction of background from cosmic rays and beam-gas interactions, the position of the primary vertex is required to be consistent with the known volume of the interaction point and the time difference between scintillator hits on opposite sides of the detector is required to be consistent with tracks originating at the interaction point.

### B. Decay mode identification

The criteria for identification of  $e$ ,  $\mu$ ,  $\pi$ , and  $\rho$  in this analysis are described below. It is required that the polar angle satisfy  $|\cos\theta| < 0.9$  unless specified otherwise. Further details can be found in Ref. 6.

#### Electrons

The signature for an electron is a charged track in the central drift chamber associated with a single shower in the electromagnetic portions of the calorimeters (EMC). Only electrons satisfying  $|\cos\theta| < 0.75$  are included in the analysis, since the event selection criteria are not efficient for low angle electrons (due to the cuts needed to reject the large number of events from the Bhabha scattering and 2-photon processes). The specific identification requirements are:

- CD momentum  $> 1$  GeV/c;
- $\geq 90\%$  of track-associated calorimeter energy contained in the EMC;
- Azimuthal angle between CD track and associated shower  $< 2^\circ$ ;

- Rms azimuthal width of associated shower  $< 4^\circ$ ;
- No additional shower ( $E > 500$  MeV) within  $65^\circ$  of CD track;
- Track hadronic energy  $< 10\%$  of track momentum;
- No energy in the outer layer of the hadron calorimeters; and
- No OD track associated with the CD track.

These criteria select electrons with efficiency  $\gtrsim 90\%$  for momenta above  $2$  GeV/ $c$ , as measured with pure electron samples from the processes  $e^+e^- \rightarrow e^+e^-$  and  $e^+e^- \rightarrow e^+e^-e^+e^-$ . The background in the electron sample is predicted by the Monte Carlo simulation to be  $10\%$ , mostly from  $\tau \rightarrow \nu_\tau\rho$ .

### Muons

A muon is recognized by the presence of a track in the outer drift chambers associated with a CD track, and energy deposition in the calorimeters consistent with that of a minimum ionizing (minI) particle. A charged track is identified as a muon if the following criteria are satisfied:

- CD momentum  $> 2$  GeV/ $c$ ;
- Acceptable  $\chi^2$  for fit to common CD/OD track;
- EMC energy consistent with minI track ( $< 1$  GeV); and
- Hadronic calorimeter energy consistent with minI track ( $< 6$  GeV).

The efficiency for these cuts is about  $85\%$ , nearly independent of polar angle and momentum, as measured with events from the process  $e^+e^- \rightarrow e^+e^-\mu^+\mu^-$ . The background in the muon sample is predicted by the Monte Carlo to be  $3\%$ , almost entirely from  $\tau \rightarrow \nu_\tau\pi$ .

## Pions

The signature for a pion is a shower in the hadron calorimeters with energy consistent with the CD track momentum. The pion identification requirements were the following:

- CD momentum  $> 2 \text{ GeV}/c$ ;
- $\geq 25\%$  of track-associated calorimeter energy in the hadron calorimeters;
- Energy in the 1st layer of EMC consistent with minI track;
- No additional shower within  $50^\circ$  of CD track;
- CD track extrapolates to an active area of the OD; and
- No OD track associated with the CD track.

Due to these harsh requirements, necessitated by the relatively large branching fractions for the modes  $\tau \rightarrow \nu_\tau \mu \bar{\nu}_\mu$  and  $\tau \rightarrow \nu_\tau \rho$ , the efficiency of pion identification is only 27%, independent of momentum and polar angle for  $|\cos \theta| < 0.7$ . This efficiency is estimated from the Monte Carlo since there is no background-free source of high-momentum pions in the data. The background is estimated to be 10%, dominated by the process  $\tau \rightarrow \nu_\tau \rho$ .

## Rho mesons

A charged  $\rho$  is recognized by the presence of a charged track in the central drift chamber and an unassociated electromagnetic shower. Specifically, we require:

- CD momentum  $> 0.5 \text{ GeV}/c$ ;

- Track associated energy in the first layer of EMC consistent with mini track;
- An additional shower with  $E > 500$  MeV within  $50^\circ$  of CD track;
- No other showers ( $E > 100$  MeV) within  $50^\circ$  of CD track; and
- No OD track associated with the CD track.

The efficiency for  $\rho$  identification is  $\sim 45\%$  for most momenta and angles, though it is somewhat dependent on both. The Monte Carlo provides the only estimate of the  $\rho$  identification efficiency. The background is estimated to be 25%, mostly from tau 1-prong decays with multiple  $\pi^0$ 's.

Additional discussion of efficiencies and backgrounds and the systematic errors associated with them will be found in section IV.B.1

### C. Monte Carlo simulation

Monte Carlo techniques are used to calculate the tau-pair selection efficiency and particle misidentification and non-tau background levels. The simulation of the experiment consists of four steps.

1. The reaction  $e^+e^- \rightarrow \tau^+\tau^-$  is simulated with the lepton-pair generator written by Berends, Kleiss, and Jadach (BKJ),<sup>8</sup> based on their calculations of the process  $e^+e^- \rightarrow \mu^+\mu^-$  to order  $\alpha^3$ , but modified to exclude the lowest order weak terms.
2. The output of step 1 serves as input to the tau decay simulation, based on a calculation of the spin dependent cross section for tau-pair production in  $e^+e^-$  annihilation.<sup>3</sup> Monte Carlo event weights are renormalized to

account for the fact that the production cross section has already been determined in step 1.

3. The output of step 2 serves as input to a simulation of the detector. Electromagnetic showers are simulated by the EGS code<sup>9</sup> and hadronic showers and minimum ionizing particle propagation are simulated by the High Energy Transport Code (HETC).<sup>10</sup> These programs trace primary and secondary particles through a detailed description of the composition, geometry, and segmentation of the detector (particles are traced until their energies are less than 5 MeV). The results of the HETC and EGS simulations are used to calculate positions and pulse heights of calorimeter and scintillator hits and positions of drift chamber hits for the OD and CD. This information is digitized and saved in files with the same structure as the real data. After the detector response to an event is recorded, the hardware trigger is simulated.
4. From this point on, the Monte Carlo data and the real data are analysed with the same programs. The input Monte Carlo momenta (output of step 2) are available for each event during the analysis.

To study background reactions, steps 1 and 2 above are replaced by event generators based on calculations by Sjöstrand<sup>11</sup> for  $e^+e^- \rightarrow q\bar{q}$  and by Smith and co-workers<sup>12</sup> for  $e^+e^- \rightarrow e^+e^-e^+e^-$ ,  $e^+e^- \rightarrow e^+e^-\mu^+\mu^-$ ,  $e^+e^- \rightarrow e^+e^-q\bar{q}$ , and  $e^+e^- \rightarrow e^+e^-\tau^+\tau^-$  (the tau decay simulation is performed with the same program used for step 2 above). The BKJ lepton-pair generator is used for processes  $e^+e^- \rightarrow e^+e^-$  and  $e^+e^- \rightarrow \mu^+\mu^-$ .

## IV. TAU POLARIZATION

### A. Polarization measurement

The combination of a weak contribution to tau-pair production and the  $V - A$  nature of tau decay modifies the energy spectra of tau decay products. Both the average energy and the energy asymmetry are measured in this experiment and are interpreted as measurements of the average tau polarization and polarization asymmetry, respectively. Since the PEP beams are not polarized,<sup>13</sup> the only source of tau polarization comes from weak production and therefore this experiment yields measurements of the products  $g_v^e g_a^r$  and  $g_a^e g_v^r$ . Since  $g_a^r$ ,  $g_v^e$ , and  $g_a^e$  have been measured more precisely elsewhere,<sup>14-21</sup> the focal point of this experiment is to measure the polarization asymmetry to determine  $g_v^r$ . The accuracy of the average polarization measurement is limited by systematic effects, whereas the precision of the polarization asymmetry is limited only by statistics, since there is cancellation of most systematic effects.

The average energy as a function of polar angle  $\bar{E}(\theta)$  can be calculated from the differential decay rates given in section I and can be written in the form

$$\bar{E}(\theta) = E_{beam} [a + b P(\theta)], \quad (15)$$

where  $E_{beam}$  is the beam energy,  $P$  is the polarization, and  $a$  and  $b$  are constants which are characteristic of a particular decay mode. It follows that the energy and energy asymmetry averaged over polar angle,  $\langle E \rangle$  and  $A_E$  respectively, are

$$\langle E \rangle = E_{beam} (a + b \langle P \rangle) \quad (16)$$

$$A_E = b E_{beam} A_P. \quad (17)$$

The energy asymmetry is defined by  $A_E = (\langle E \rangle_F - \langle E \rangle_B)/2$ , where  $\langle E \rangle_F$  and  $\langle E \rangle_B$  are the average energies for  $\cos \theta > 0$  and  $\cos \theta < 0$ , respectively. Radiative corrections to tau-pair production reduce the average tau energy and also introduce a small energy asymmetry to the taus. To account for these corrections and other effects such as momentum acceptance, solid angle acceptance (in the case of the polarization asymmetry), particle identification, and non-tau backgrounds, it is convenient to write Eqs. (16) and (17) in terms of the weak coupling constants and the corresponding effective coefficients,

$$\langle E \rangle = E_{beam} (a' + b' g_a^\tau g_v^e) \quad (18)$$

$$A_E = b'' E_{beam} g_a^e g_v^\tau + \delta_A. \quad (19)$$

Table 1 lists the measured average energies and energy asymmetries for the four decay modes used in this analysis and the Monte Carlo predictions for the standard model (i.e.,  $V - A$  tau decays, massless neutrinos,<sup>22</sup> the values of weak coupling constants measured in other experiments, and the values of branching fractions reported as of 1984<sup>23</sup>). The central drift chamber momenta are used for energy measurements except in the case of  $\tau \rightarrow \nu_\tau \rho$  decays for which it is necessary to use the EMC to measure the  $\pi^0$  energy.<sup>24</sup> To reduce the effect of the small fraction of decays with very large measured momenta ( $p \gg E_{beam}$ ) on the means and widths of the momentum spectra, the spectra are truncated at 20 GeV/c. The Monte Carlo predictions in Table 1 include the effects of backgrounds and efficiencies. The values of measured  $\langle E \rangle$  and  $A_E$  are corrected

for effects from non-tau backgrounds; the background fractions are less than 3% and the results are insensitive to these corrections. The values of the energy spectrum parameters  $a$  and  $b$  are also listed in Table 1 along with the effective energy spectrum parameters  $a'$ ,  $b'$ ,  $b''$ , and  $\delta_A$ .

Figures 2 and 3 show the  $\cos \theta$  and momentum distributions for the four decay channels. The observed distributions are compared with the Monte Carlo predictions (not including non-tau backgrounds which are negligible). The bin-to-bin fluctuations in the Monte Carlo predictions are due to the limited statistics of the Monte Carlo sample. The structure seen in the  $\cos \theta$  distribution of Fig. 2c is due to the non-uniformity of the outer drift chamber coverage. The excellent agreement between the data and the Monte Carlo predictions of the  $\cos \theta$  distributions for the four decay modes indicates that the effective coefficients  $b''$  have been computed with the correct  $\cos \theta$  dependence for the  $3x^2/(3x + x^3)$  factor in Eq. (7). The Monte Carlo and observed momentum spectra are in good agreement except for the decay  $\tau \rightarrow \nu_\tau \rho$  (Fig. 3d). This discrepancy will be discussed in section IV.B.1.

The Monte Carlo sample used to calculate the quantities in Table 1 corresponds to an integrated luminosity of  $1200 \text{ pb}^{-1}$  (about six times that of the data) and was created with a record of all information needed to re-weight events with different values of the weak coupling constants. This allows measurement of the sensitivity of a particular effect to changes in the coupling constants. Since the axial-vector couplings have been measured with much better precision than the current measurements of the vector couplings, it is assumed that the former are known and only the vector coupling constants are varied. The average ener-

gies and energy asymmetries are linear functions of the coupling constants over their full range of values. Since the sensitivity factors  $b'$  and  $b''$  are determined by variation of the vector coupling constants, their statistical errors are negligible.<sup>25</sup>

## B. Systematic uncertainties

Detailed estimates of a variety of systematic effects are described in the following sections. There are generally two types of contributions to the systematic error, those which represent a shift of the energy scale and those which are a multiplicative scale factor. The former are important for the mean polarization analysis but cancel for the polarization asymmetry, but the latter contribute to both. A more detailed discussion can be found in Ref. 6.

### 1. Background levels and detection efficiencies

Since both the average energy and the sensitivity to the tau polarization are dependent upon the decay channel, it is important to know the amount of misidentification and non-tau background in each channel. Misidentification of leptons as hadrons and vice versa is especially troublesome since their polarization dependencies have opposite signs. Signal to background ratios are affected by branching fractions, detection efficiency, and background rejection inefficiency. Incorrect modeling of the momentum dependence of detection efficiencies is a potential source of bias to the average energy.

In Table 2 we give estimates for the systematic errors in  $a'$ ,  $b'$ , and  $b''$ , due to uncertainty in tau branching fractions. Note that the errors for the hadronic modes are larger than for the leptonic modes. The large contribution to  $\delta\langle E \rangle_\rho$  is due to the large uncertainty in the fraction of events with more than one  $\pi^0$  and

the inability of the detector to resolve the multiple  $\pi^0$ 's. Only the largest single background is included in the table since others have relatively small effects.

The estimated systematic error in  $a'$  due to incorrectly modeled energy dependence of the detection efficiencies is given in Table 3. Also given in the table are estimates of the systematic errors in  $b'$  and  $b''$  caused by uncertainties in the background levels and the average efficiencies. The systematic errors assigned for the  $\rho$  decay mode are particularly large mainly because the average energies, measured separately for charged and neutral particles, are not well reproduced by the Monte Carlo and these differences are quite dependent on the requirements used to define a neutral shower in the SC. Another source of systematic error for the decay mode  $\tau \rightarrow \nu_\tau \rho$  is uncertainty in the absolute energy calibration of the SC. After detailed studies of Bhabha scattering events,<sup>26</sup> we assign a conservative systematic error of 2% to the average neutral energy in  $\tau \rightarrow \nu_\tau \rho$  decays (1% in  $\langle E \rangle_\rho$ ).

## 2. Energy resolution and calibration

Because the resolution of the CD is Gaussian in inverse momentum rather than momentum, the resolution smearing is not symmetric about the true momentum and causes a bias in  $\langle p \rangle$  which depends on the energy spectrum and how the high-momentum tail is treated. Variation of the truncation point (described in section IV.A) by  $\pm 5$  GeV/c is used to estimate the systematic errors introduced by the truncation procedure and any differences between the data and Monte Carlo. These estimates are included in Table 3. Also included in the table are estimates of the systematic error due to incorrect calibration of the

CD momenta, assumed to be due to uncertainty in the solenoid magnetic field. These were determined by a comparison of the data and Monte Carlo momentum distributions of Bhabha scattering and mu-pair events.

### 3. Detector energy asymmetries

Due to causes which are not well understood, the signed CD inverse-momentum spectrum is not symmetric around zero. We fit the inverse momentum spectrum of tracks from the process  $e^+e^- \rightarrow \mu^+\mu^-$  to determine that the shift in  $1/p$  is  $-0.0075 \pm 0.0011$  (GeV/c) $^{-1}$ . The flat pion momentum spectrum is most susceptible to this shift since higher momentum tracks are shifted more ( $\delta p = p^2\delta(1/p)$ ). We correct for this effect in the data by the addition of 0.0075 GeV/c to the inverse momentum of each CD track and assign a systematic error of half the size of the shift for  $\langle E \rangle$  (0.1% for  $e$  and  $\mu$ , 0.3% for  $\pi$ , and 0.1% for  $\rho$ ). Actual physical energy asymmetries of the detector have been considered and found to be negligible.

A misidentification of the charge of both tracks would dilute the energy asymmetry. However, the fraction of events in the two-prong tau data with two tracks of the same charge is about 3% and the estimated fraction of events with two charge misidentifications is about 1%. A systematic error of 1% is assigned to the energy asymmetry of all four decay modes since the Monte Carlo did not accurately predict the amount of charge misidentification in mu-pair samples.

### 4. Radiative corrections to tau production

Since initial state radiation affects only the electron from which it is radiated, it cannot cause the spin of a tau to flip. Depolarization due to the flipping of the

spin of a high energy tau by final state radiation is also negligible by approximate helicity conservation for high-energy Dirac fermion currents.<sup>27</sup>

The effects of soft bremsstrahlung and vertex corrections to order  $\alpha^3$  are estimated with the calculations of Böhm and Hollik.<sup>28</sup> At  $\sqrt{s} = 29$  GeV these corrections decrease the average polarization by  $\sim 2\%$  when the maximum allowed radiated photon energy is less than 20% of the beam energy. Figure 4 shows the polarization with and without radiative corrections as a function of polar angle. Since these effects are far smaller than the sensitivity of this experiment, they are ignored.

Although radiative corrections have little effect on the polarization, radiation reduces the energy of the taus and therefore also the average energy of the tau decay products. Radiative corrections also produce a small energy asymmetry of the taus themselves. Corrections are made to the energy measurement parameters listed in Table 1. The ability of the BKJ event generator to model the data has been checked in the reaction  $e^+e^- \rightarrow \mu^+\mu^-(\gamma)$  for events without<sup>29</sup> and with<sup>30</sup> an observed photon with energy greater than 1 GeV. Also the charge asymmetry in radiative events from the process  $e^+e^- \rightarrow \tau^+\tau^-\gamma$  has been measured and found to be in agreement with the BKJ Monte Carlo prediction.<sup>19</sup>

From the agreement of the BKJ calculations and event generator with the data, we estimate that the systematic errors could be at most 10% of the size of the radiative effects. Since  $\langle E \rangle$  scales directly with the tau energy and the average tau energy is 96.6% of the beam energy, a systematic error of  $(1 - 0.966) \times 10\% = 0.34\%$  is assigned for  $\langle E \rangle$  in all four channels.

## 5. Radiative corrections to tau decay

Radiative corrections to the differential decay rate for the decay  $\mu \rightarrow \nu_\mu e \bar{\nu}_e$  have been calculated and can be applied directly to leptonic tau decays.<sup>31</sup> The calculation, which includes virtual and bremsstrahlung diagrams, was carried out to order  $\alpha^3$ . The results of this calculation are used to estimate the effect of radiative corrections on the measured  $\langle E \rangle$  and the sensitivity to the polarization. When integrated over the energy spectrum and solid angle, these radiative corrections change the average energy and energy asymmetry for electrons (muons) by about 1.5% (0.4%). Since the masses of the  $\pi$  and  $\rho$  are larger than the  $\mu$  mass, the corrections to these decay modes are negligible. We correct measured  $\langle E \rangle$  and  $A_E$  since the decay radiative corrections were not originally implemented in the Monte Carlo event generator. Conservative systematic errors, assigned as half the difference between the corrections with and without inclusion of the approximate momentum acceptance, are given in Table 3.

## 6. Beam Energy

The beam energy was 14.5 GeV during the entire data collection period. The energy of the beams is determined by the integral of the bend magnetic fields around the PEP ring.<sup>32</sup> We estimate the total error on the absolute calibration of the beam energy to be less than 0.05%. The amount of beam wandering due to changing orbits is less than 0.2% and the width of the beam energy distribution is 0.1%. The total systematic error attributed to the knowledge of the beam energy is 0.1%.

### C. Summary of tau polarization results

With the assumption of standard  $V - A$  tau decays, the energy spectra for the four decay modes can be used to find the average tau polarization and polarization asymmetry (extrapolated to full acceptance assuming the polarization to be of the form  $c_1 + c_2 \times 2 \cos \theta / [1 + \cos^2 \theta]$ ):

$$\langle P \rangle = -0.02 \pm 0.07 \pm 0.11$$

$$A_P = (0.06 \pm 0.07) \times (1 \pm 0.011),$$

where the first errors are statistical and the second are systematic and the multiplicative systematic errors are indicated as product errors. The calculation of the systematic errors accounts for the fact that many uncertainties are common to all decay modes, but the largest are not. These results are consistent with the predictions of the GWS model,  $\langle P \rangle = 0.0101$  and  $A_P = 0.0076$ . From Eqs. (6) and (7), we find the coupling constant products to be

$$g_v^e g_a^\tau = -0.05 \pm 0.21 \pm 0.34$$

$$g_a^e g_v^\tau = (0.26 \pm 0.31) \times (1 \pm 0.011).$$

The measured coupling constant products for the individual decay modes are shown in Table 4. In the GWS model the values of the axial-vector couplings of the electron and tau to the weak neutral current are both  $-1/2$ . With this assumption we find

$$g_v^e = 0.10 \pm 0.42 \pm 0.68$$

$$g_v^\tau = (-0.52 \pm 0.62) \times (1 \pm 0.011).$$

## V. COUPLING OF $\tau \nu_\tau$ TO WEAK CHARGED CURRENT

Since there is abundant evidence from  $\mu$  decay and other weak processes that  $e \bar{\nu}_e$  and  $\mu \bar{\nu}_\mu$  have purely  $V - A$  coupling to the weak charged current, the only uncertainty in the Lorentz structure of tau decay is the coupling at the  $\tau \bar{\nu}_\tau - W$  vertex. If the coupling at this vertex is written as

$$\alpha(V - A) + \beta(V + A) \quad (20)$$

the Michel parameter becomes<sup>33</sup>

$$\rho = \frac{3}{4} \left( 1 - \frac{\beta^2}{\alpha^2 + \beta^2} \right). \quad (21)$$

Interactions which are pure  $V - A$ ,  $V$  or  $A$ ,  $V + A$  give  $\rho = \frac{3}{4}$ ,  $\frac{3}{8}$ , and 0, respectively.

In terms of the Michel parameter, the differential decay rates for the four decay modes considered here, neglecting all masses apart from the  $\rho$  mass (where the narrow width approximation has been made) are

$$\begin{aligned} \frac{d^2 \Gamma_{e, \mu}}{dx d \cos \theta} &= \frac{G_F^2 m_\tau^5}{192 \pi^3} \frac{2}{3} \left\{ 9x^2(1-x) + 2\rho x(4x^2 - 3x) \right. \\ &\quad \left. + P \cos \theta \left( 3 - \frac{8}{3}\rho \right) x \right. \\ &\quad \left. \times \left[ 3x(1-x) + \frac{3}{2} \left( 1 - \frac{3-4\rho}{3-\frac{8}{3}\rho} \right) x(4x-3) \right] \right\}, \\ \frac{d\Gamma_\pi}{d \cos \theta} &= \frac{G_F^2 f_\pi^2 \cos^2 \theta_c}{32 \pi} m_\tau^3 \left( 1 - \frac{m_\pi^2}{m_\tau^2} \right)^2 \\ &\quad \times \left[ 1 + P \cos \theta \left( \frac{8}{3}\rho - 1 \right) \right], \text{ and} \\ \frac{d\Gamma_\rho}{d \cos \theta} &= \frac{G_F^2 f_\rho^2 \cos^2 \theta_c}{32 \pi} \frac{m_\tau^3}{m_\rho^2} (1-y)^2 (1+2y) \\ &\quad \times \left[ 1 + P \cos \theta \frac{1-2y}{1+2y} \left( \frac{8}{3}\rho - 1 \right) \right] \end{aligned} \quad (22)$$

where  $y = m_\rho^2/m_\tau^2$ . It is then a simple matter to show that the average energies

in the laboratory are

$$\begin{aligned}
\langle E \rangle_{e,\mu} &\simeq E_{beam} \left( \frac{2\rho + 9}{30} + P \frac{1 - \frac{2}{3}\rho}{10} \right), \\
\langle E \rangle_{\pi} &\simeq E_{beam} \left( \frac{1}{2} + P \frac{\frac{8}{3}\rho - 1}{6} \right), \text{ and} \\
\langle E \rangle_{\rho} &\simeq E_{beam} (1 + y) \left( \frac{1}{2} + \frac{P \left( \frac{8}{3}\rho - 1 \right) (1 - 2y)}{6(1 + 2y)} \right).
\end{aligned} \tag{23}$$

Note that for hadronic  $\tau$  decays only the polarization dependent terms of  $\langle E \rangle$  depend on  $\rho$ , in contrast with the leptonic decays for which there is  $\rho$  dependence in both the constant and polarization dependent terms of  $\langle E \rangle$ .

The polarization experiment consists in part of measuring the average laboratory energy. The average energy also can be used to measure  $\rho$  if it is assumed that the tau polarization is small as expected in the GWS model. Only the leptonic decay modes are used, since the average energy in hadronic tau decays is not sensitive to  $\rho$ .<sup>34</sup>

The Monte Carlo is used to calculate the  $\rho$  dependence of the average laboratory energy for the leptonic decay modes. The calculated coefficients  $a_{e,\mu}$  and  $b_{e,\mu}$ , defined by

$$\langle E \rangle_{e,\mu} = a_{e,\mu} + b_{e,\mu} \left( \rho - \frac{3}{4} \right), \tag{24}$$

are given in Table 5 along with the measured values of  $\langle E \rangle_{e,\mu}$ . The effects of particle misidentification on  $a_{e,\mu}$  (a bias) and  $b_{e,\mu}$  (decreased sensitivity) have been included. Figure 5 shows the electron and muon momentum spectra compared with the Monte Carlo for extreme values of  $\rho$ . The description of the contributions to the systematic errors in  $\langle E \rangle$  are described in section IV.B and can be

applied directly here. The final results are

$$\rho_e = 0.62 \pm 0.17 \pm 0.14$$

$$\rho_\mu = 0.89 \pm 0.14 \pm 0.08,$$

where the first errors are statistical and the second are systematic.

## VI. SUMMARY AND DISCUSSION

The experimental values for the average polarization and polarization asymmetry, obtained from measurements of the mean energy and energy asymmetry of decay products of taus produced in  $e^+e^- \rightarrow \tau^+\tau^-$ , are

$$\langle P \rangle = -0.02 \pm 0.07 \pm 0.11$$

$$A_P = (0.06 \pm 0.07) \times (1 \pm 0.011).$$

These results are consistent with the predictions of the GWS model,  $\langle P \rangle = 0.0101$  and  $A_P = 0.0076$ . From these values, the weak neutral current coupling constant products are measured to be

$$g_v^e g_a^\tau = -0.05 \pm 0.21 \pm 0.34$$

$$g_a^e g_v^\tau = (0.26 \pm 0.31) \times (1 \pm 0.011).$$

The value of the axial-vector coupling of the electron to the weak neutral current in the GWS model is  $-1/2$ . With this assumption, the measured  $g_a^e g_v^\tau$  yields

$$g_v^\tau = (-0.52 \pm 0.62) \times (1 \pm 0.011).$$

This result is considerably more precise than that reported by the CELLO collaboration,<sup>35</sup>  $2g_v^\tau = -0.1 \pm 2.8$ , also determined with the polarization

asymmetry technique. Both the present result and that reported by CELLO are consistent with the values expected in the GWS model, but the errors are too large to make any serious tests of lepton universality. It should be noted that the only other measurements of  $g_v^\tau$  have been made by comparison of the total cross section for the process  $e^+e^- \rightarrow \tau^+\tau^-$  with the QED cross section. This is also a difficult experiment since the effect is proportional to  $g_v^e g_v^\tau$  and  $g_v^e$  is known to be small ( $-0.05 \pm 0.09$ ).<sup>21</sup> A recent measurement by the Mark J collaboration<sup>36</sup> yields  $g_v^\tau = 0.0 \pm 1.8$  when the above value for  $g_v^e$  is used.

A measurement of the Michel parameter  $\rho$  is also presented, obtained from the energy spectra of leptonic tau-decay products, with the assumption that the tau polarization is indeed small as expected from the GWS model. The observed values for the tau decays  $\tau \rightarrow \nu_\tau e \bar{\nu}_e$  and  $\tau \rightarrow \nu_\tau \mu \bar{\nu}_\mu$  are

$$\rho_e = 0.62 \pm 0.17 \pm 0.14$$

$$\rho_\mu = 0.89 \pm 0.14 \pm 0.08,$$

respectively. Since the couplings of  $e \bar{\nu}_e$  and  $\mu \bar{\nu}_\mu$  to the  $W$  have been shown to be the same, these results can be combined to yield

$$\rho = 0.79 \pm 0.10 \pm 0.10.$$

The results presented here are in good agreement with previous measurements of the Michel  $\rho$  parameter included in Table 6. When combined with previous results, the new world average becomes  $\rho = 0.73 \pm 0.07$ .  $V + A$ ,  $V$ , or  $A$  interactions at the  $\tau \bar{\nu}_\tau$ - $W$  vertex are ruled out, but only admixtures of more than 47%  $V + A$  with the expected  $V - A$  interaction can be excluded with 95% confidence by the combined results.

The support of the SLAC staff, and in particular the PEP operators, is gratefully acknowledged.

## REFERENCES

- (a) Present address: University of Oslo, N-0316 Oslo 3, Norway.
  - (b) Present Address: CERN, Geneva, Switzerland.
  - (c) Present Address: Texas Accelerator Center, The Woodlands, Texas 77380.
  - (d) Permanent address: CERN, Geneva, Switzerland.
  - (e) Present Address: Enrico Fermi Institute, University of Chicago, Chicago, Illinois 60637.
  - (f) Present address: Universidad Autónoma de Barcelona, Barcelona, Spain.
1. S. Weinberg, Phys. Rev. Lett. **19**, 1264 (1967); A. Salam, *Elementary Particle Theory*, edited by N. Svartholm (Almqvist and Forlag, Stockholm, 1968), p. 367; G. t'Hooft, Nucl. Phys. B **35**, 167 (1971); B. W. Lee, Phys. Rev. D **5**, 823 (1972); S. Weinberg, Phys. Rev. Lett. **27**, 1688 (1971).
  2. M. Aguilar-Benitez *et al.* (Particle Data Group), Phys. Lett. **170B** (1986).
  3. H. D. Dahmen, L. Schülke, and G. Zech, Z. Physik C **5**, 71 (1980).
  4. G. Arnison *et al.* (UA-1 Collaboration), Phys. Lett. **122B**, 103 (1983); M. Banner *et al.* (UA-2 Collaboration), Phys. Lett. **122B**, 476 (1983).
  5. See, for instance, E. Fernandez *et al.* (MAC Collaboration), Phys. Rev. D **31**, 1537 (1985) and references therein.
  6. A. L. Read, Univ. of Colorado-Boulder Ph.D. Thesis, Report COLO-HEP-122 (1986).

7. Actually kaons are also included since the MAC detector has no  $\pi/K$  separation capabilities. This is not a problem since the branching fraction  $B_K$  has been measured and found to be only  $\sim 6\%$  of  $B_\pi$ .
8. F. A. Berends, R. Kleiss, and S. Jadach, Nucl. Phys. B **202**, 63 (1982).
9. R. L. Ford and W. R. Nelson, SLAC Report No. SLAC-PUB-210, unpublished (1978).
10. T. W. Armstrong, in *Computer Techniques in Radiation Transport and Dosimetry*, edited by W. R. Nelson and T. M. Jenkins (Plenum, New York, 1980).
11. T. Sjöstrand, Comput. Phys. Commun. **27**, 243 (1983).
12. R. Bhattacharya, J. Smith, and G. Grammer, Jr., Phys. Rev. D **15**, 3267 (1977); J. Smith, J. A. M. Vermaseren, and G. Grammer, Phys. Rev. D **15**, 3280 (1977).
13. The uncompensated magnets of the various PEP detectors destroy any transverse polarization which develops.
14. E. Fernandez *et al.* (MAC Collaboration), Phys. Rev. Lett. **54**, 1620 (1985).
15. M. E. Levi *et al.* (Mark II Collaboration), Phys. Rev. Lett. **51**, 1941 (1983).
16. W. Bartel *et al.* (JADE Collaboration), Phys. Lett. **161B**, 188 (1985).
17. K. K. Gan *et al.* (HRS Collaboration), Phys. Lett. **153B**, 116 (1985).
18. Ch. Berger *et al.* (PLUTO Collaboration), Z. Physik C **28**, 1 (1985).
19. M. Althoff *et al.* (TASSO Collaboration), Z. Physik C **26**, 521 (1985).

20. E. Fernandez *et al.* (MAC Collaboration), Phys. Rev. D **35**, 10 (1987).
21. F. Reines, H. S. Gurr, and H. W. Sobel, Phys. Rev. Lett. **37**, 315 (1976);  
F. T. Avignone *et al.*, Phys. Rev. D **16**, 2383 (1977); W. Krenz, Physikalisches Institut, Technische Hochschule Aachen, Germany preprint PITHA 82/26 (1982, unpublished).
22. The current upper limit on the  $\tau$  neutrino mass is  $70 \text{ MeV}/c^2$  from H. Albrecht *et al.* (ARGUS Collaboration), Phys. Lett. **163B**, 404 (1985); see also S. Abachi *et al.* (HRS Collaboration), Phys. Rev. Lett. **56**, 1039 (1986).  
The systematic error introduced by this assumption is negligible.
23. C. G. Wohl *et al.* (Particle Data Group), Rev. Mod. Phys. **56**, S1 (1984).
24. The weighted average of the CD and OD momenta are actually used for the muon energy asymmetry measurement, but not  $\langle E \rangle$ , since the associated systematic errors largely cancel.
25. The distributions of  $b'$  and  $b''$ , for ten equal subsamples of the Monte Carlo sample, indicate that the statistical errors on these quantities are less than 3%.
26. M. C. Delfino, Univ. of Wisconsin-Madison Ph.D. Thesis, Report WISC-EX-85/263 (1985).
27. See, for example, *Quarks and Leptons: An Introductory Course in Modern Particle Physics* by F. Halzen and A. D. Martin, pp. 126-127, N.Y., Wiley, (1984).
28. M. Böhm and W. Hollik, Nucl. Phys. B **204**, 45 (1982); W. Hollik, University of Würzburg Print-83-0312 (unpublished).

29. E. Fernandez *et al.* (MAC Collaboration), Phys. Rev. Lett. **50**, 1238 (1983).
30. W. T. Ford *et al.* (MAC Collaboration), Phys. Rev. Lett. **51**, 257 (1983).
31. T. Kinoshita and A. Sirlin, Phys. Rev. **113**, 1652 (1958); F. Scheck, Phys. Reports **44**, 187 (1978); A. Ali and Z. Z. Aydin, Nuovo Cim. **43A**, 270 (1978).
32. G. E. Fisher, SLAC technical note PEP-PTM-210, 1979 (unpublished); R. H. Helm, P. B. Wilson, and H. Wiedemann, SLAC technical note PEP-PTM-103-R1, 1975 (unpublished); J. Martin, private communication.
33. K. Mursula and F. Scheck, Nucl. Phys. B **253**, 189 (1985).
34. For hadronic tau decays, angular or energy correlations of the two tau decay products can, in principle, be used to test the  $V - A$  nature of the interaction. See for instance J. Babson and E. Ma, Phys. Rev. D **26**, 2497 (1982); J. Babson and E. Ma, Z. Physik C **20**, 5 (1983).
35. H. J. Behrend *et al.* (CELLO Collaboration), Phys. Lett. **127B**, 270 (1983).
36. B. Adeva *et al.* (MARK J Collaboration), Phys. Lett. **179B**, 177 (1986).

## FIGURE CAPTIONS

1. Feynman diagrams for lowest order cross section for the process  $e^+e^- \rightarrow \tau^+\tau^-$ .
2. Observed  $\cos \theta$  distribution for: a)  $\tau \rightarrow \nu_\tau e \bar{\nu}_e$ , b)  $\tau \rightarrow \nu_\tau \mu \bar{\nu}_\mu$ , c)  $\tau \rightarrow \nu_\tau \pi$ , d)  $\tau \rightarrow \nu_\tau \rho$ . The solid curves show the Monte Carlo prediction and the dotted curves show the particle misidentification background.
3. Momentum spectra for: a)  $\tau \rightarrow \nu_\tau e \bar{\nu}_e$ , b)  $\tau \rightarrow \nu_\tau \mu \bar{\nu}_\mu$ , c)  $\tau \rightarrow \nu_\tau \pi$ , d)  $\tau \rightarrow \nu_\tau \rho$ . The solid curves show the Monte Carlo prediction and the dotted curves show the particle misidentification background.
4. Polarization as function of polar angle for the expected values of the coupling constants. The dotted curve includes the effects of radiative corrections.
5. Momentum spectra for a)  $\tau \rightarrow \nu_\tau e \bar{\nu}_e$  and b)  $\tau \rightarrow \nu_\tau \mu \bar{\nu}_\mu$ . The solid (dotted) curves are the Monte Carlo predictions for the momentum spectra when  $\rho = 0.75$  ( $\rho = 0$ ).

## TABLE CAPTIONS

1. Measurements and constants for calculation of polarization (quoted errors are statistical only).
2. Systematic errors for polarization measurement due to uncertainties in tau branching fractions.
3. Summary of systematic uncertainties for quantities entering into the polarization measurement, expressed as a percentage of the listed quantity.
4. Measured coupling constant products for the individual tau decay modes.
5. Results of the Michel parameter measurement. The constants  $a_l$  and  $b_l$  (Eq. (24)) are calculated with the Monte Carlo and include the effects of background.
6. Measured values of the Michel parameter.

TABLE 1

	$\tau \rightarrow \nu_{\tau} e \bar{\nu}_e$	$\tau \rightarrow \nu_{\tau} \mu \bar{\nu}_{\mu}$	$\tau \rightarrow \nu_{\tau} \pi$	$\tau \rightarrow \nu_{\tau} \rho$
No. of obs. events	1823	1909	798	3158
$\langle E \rangle$ (GeV)	$5.58 \pm 0.10$	$6.76 \pm 0.11$	$8.51 \pm 0.20$	$8.07 \pm 0.07$
$A_E$ (GeV)	$-0.05 \pm 0.10$	$-0.06 \pm 0.09$	$-0.07 \pm 0.20$	$0.07 \pm 0.07$
$\langle E \rangle$ (GeV) pred.	$5.66 \pm 0.05$	$6.65 \pm 0.04$	$8.59 \pm 0.08$	$8.77 \pm 0.03$
$A_E$ (GeV) pred.	$0.04 \pm 0.05$	$-0.02 \pm 0.04$	$-0.07 \pm 0.08$	$-0.01 \pm 0.03$
$a$	0.35	0.36	0.50	0.60
$b$	-0.05	-0.05	0.17	0.06
$a'$	$0.390 \pm 0.003$	$0.459 \pm 0.003$	$0.590 \pm 0.005$	$0.604 \pm 0.002$
$b'$	-0.011	-0.015	0.036	0.013
$b''$	-0.005	-0.010	0.026	0.009
$\delta_A$	$0.04 \pm 0.05$	$-0.02 \pm 0.04$	$-0.07 \pm 0.008$	$-0.01 \pm 0.03$

TABLE 2.

	$\tau \rightarrow \nu_\tau e \bar{\nu}_e$	$\tau \rightarrow \nu_\tau \mu \bar{\nu}_\mu$	$\tau \rightarrow \nu_\tau \pi$	$\tau \rightarrow \nu_\tau \rho$
Dominant background	$\tau \rightarrow \nu_\tau \rho$	$\tau \rightarrow \nu_\tau \pi$	$\tau \rightarrow \nu_\tau \rho$	$\tau \rightarrow \nu_\tau A_1$
$f_{BG}$ (%)	10	3	10	25
$\delta(B/B_{BG})/(B/B_{BG})$ (%)	6	11	12	20
$ \langle E \rangle - \langle E \rangle_{BG} $ (GeV)	0.3	1.8	2.3	0.8
$\delta \langle E \rangle / \langle E \rangle$ (%)	0.1	0.1	0.4	0.6
$\delta b''$ (%)	0.8	1.0	0.5	5.0
$\delta b'' / b''$ (%)	0.7	1.0	0.4	4.0

TABLE 3.

Source	Effect	$\tau \rightarrow e$	$\tau \rightarrow \mu$	$\tau \rightarrow \pi$	$\tau \rightarrow \rho$
Common effects multiplicative in $E$ :					
EMC calibration	$a', b', b''$	-	-	-	1.0
$\sigma_{1/p}$	$a', b', b''$	1.0	0.6	0.4	0.4
Solenoid $B$ field	$a', b', b''$	0.4	0.4	0.4	0.2
Shift in $1/p$	$a', b', b''$	$< 0.1$	0.1	0.3	0.1
$\sigma_{\tau\tau}$ radiative corrections	$a', b', b''$	0.3	0.3	0.3	0.3
$\tau$ decay radiative corrections	$a', b', b''$	0.3	0.1	$\sim 0$	$\sim 0$
$E_{beam}$	$a', b', b''$	0.1	0.1	0.1	0.1
Effects for $\langle E \rangle$ measurement:					
Monte Carlo statistics	$a'$	0.8	0.6	0.9	0.3
Branching fractions	$a'$	0.1	0.1	0.4	0.6
Energy dependence of efficiency	$a'$	0.5	0.5	1.2	8.0
Branching fractions	$b'$	0.8	1.0	0.5	5.0
Efficiency, background estimate	$b'$	0.3	0.3	0.6	4.0
Effects for $A_E$ measurement:					
Branching fractions	$b''$	0.7	1.0	0.4	4.0
Efficiency, background estimate	$b''$	0.3	0.3	0.6	4.0
Charge misidentification	$b''$	1.0	1.0	1.0	1.0

TABLE 4

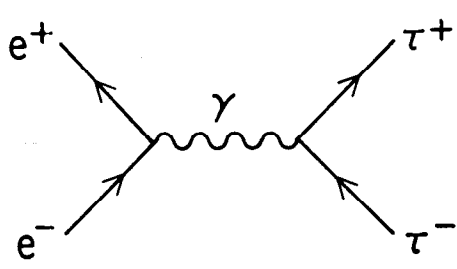
Decay mode	$g_\nu^e g_a^T$	$g_a^e g_\nu^T$
$\tau \rightarrow \nu_\tau e \bar{\nu}_e$	$0.97 \pm 0.63 \pm 0.53$	$(0.68 \pm 1.39) \times (1 \pm 0.017)$
$\tau \rightarrow \nu_\tau \mu \bar{\nu}_\mu$	$-0.53 \pm 0.50 \pm 0.35$	$(0.43 \pm 0.67) \times (1 \pm 0.017)$
$\tau \rightarrow \nu_\tau \pi$	$-0.13 \pm 0.39 \pm 0.29$	$(-0.20 \pm 0.54) \times (1 \pm 0.014)$
$\tau \rightarrow \nu_\tau \rho$	$3.54 \pm 0.34 \pm 3.34$	$(0.50 \pm 0.50) \times (1 \pm 0.059)$

TABLE 5

	electron	muon
$a_l$ (GeV)	$5.66 \pm 0.05$	$6.65 \pm 0.04$
$b_l$ (GeV)	0.61	0.78
$\langle E \rangle_l$ (GeV)	$5.58 \pm 0.10$	$6.76 \pm 0.11$

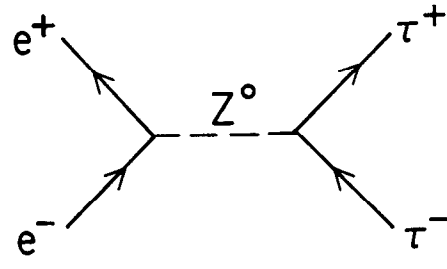
TABLE 6

Experiment	$\rho_e$	$\rho_\mu$	Average
DELCO <sup>37</sup>	$0.72 \pm 0.15$	-	$0.72 \pm 0.15$
CLEO <sup>38</sup>	$0.59 \pm 0.14$	$0.81 \pm 0.14$	$0.70 \pm 0.10 \pm 0.03$
This experiment	$0.62 \pm 0.17 \pm 0.14$	$0.89 \pm 0.14 \pm 0.08$	$0.79 \pm 0.10 \pm 0.10$
Average	$0.65 \pm 0.09$	$0.84 \pm 0.11$	$0.73 \pm 0.07$



8-86

+



5533A1

Fig. 1

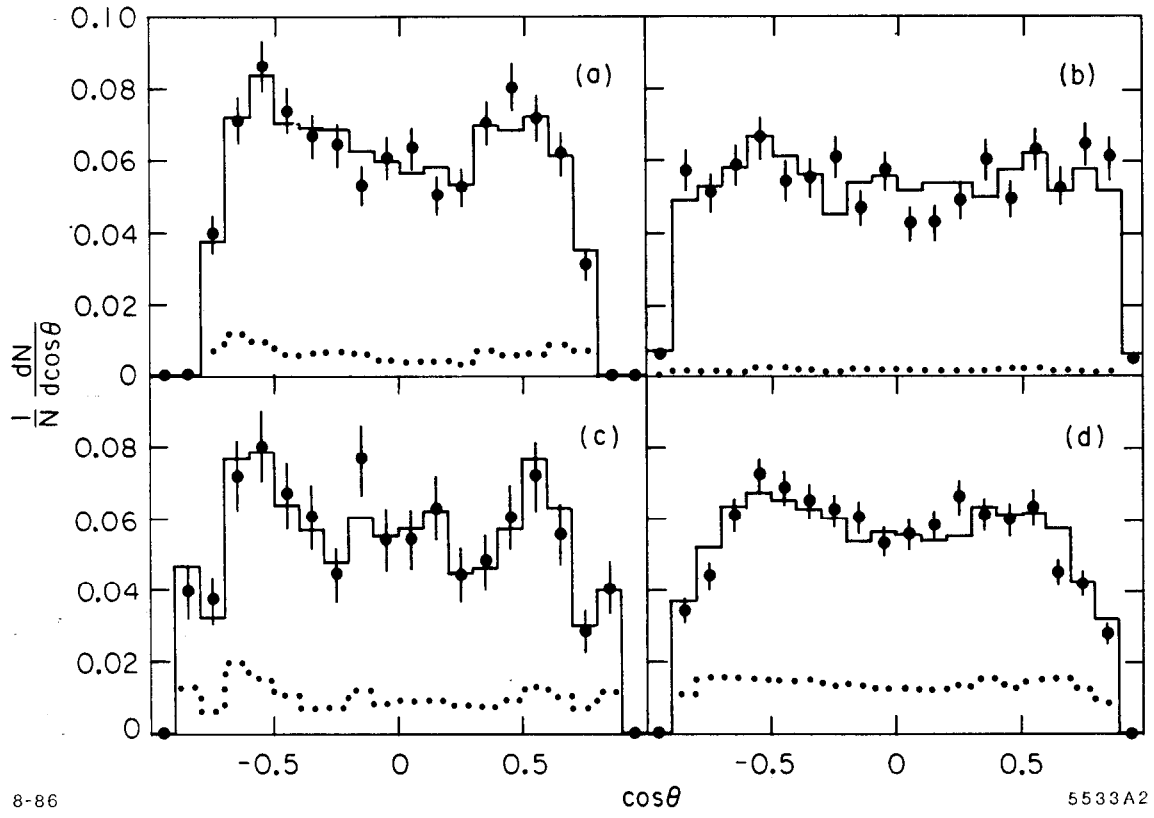


Fig. 2

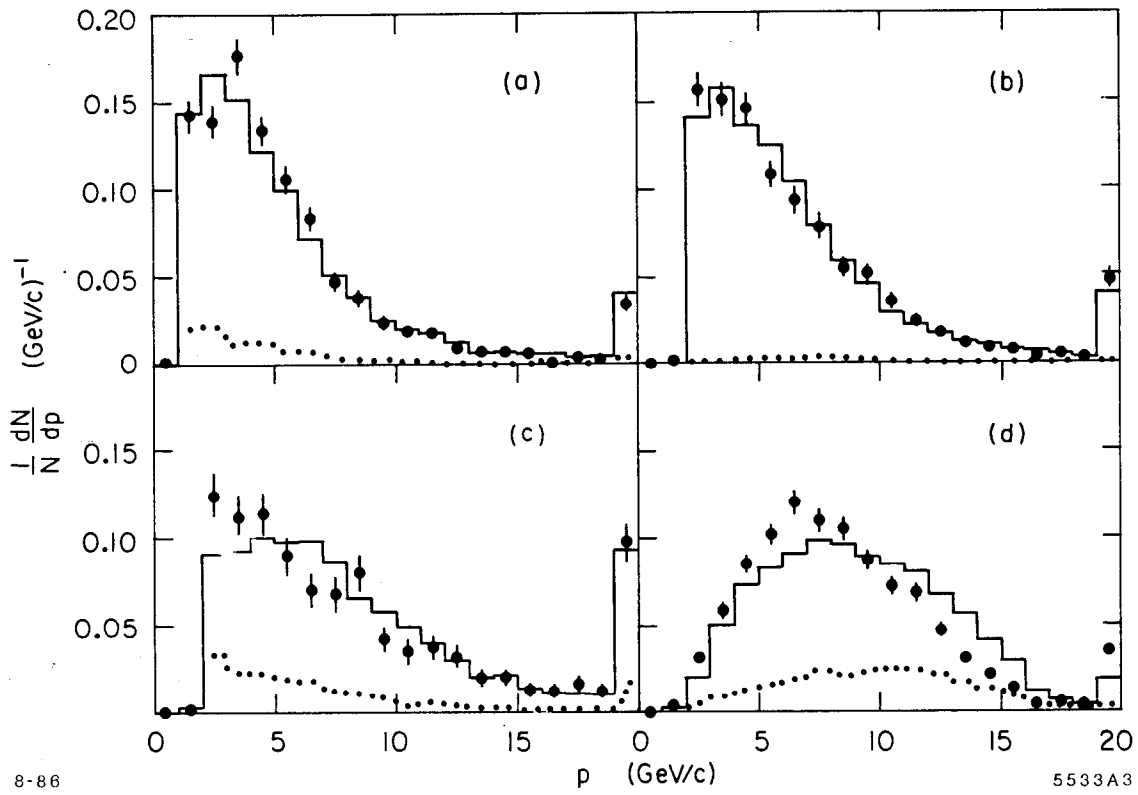


Fig. 3

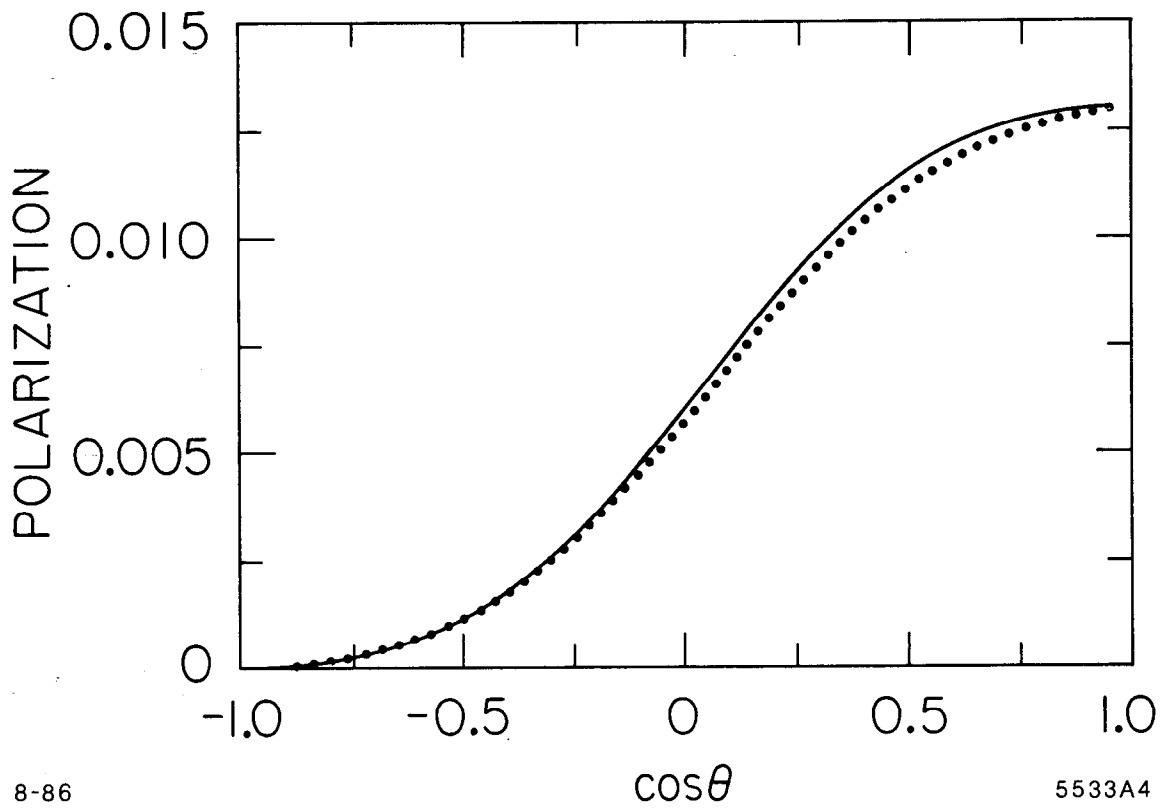
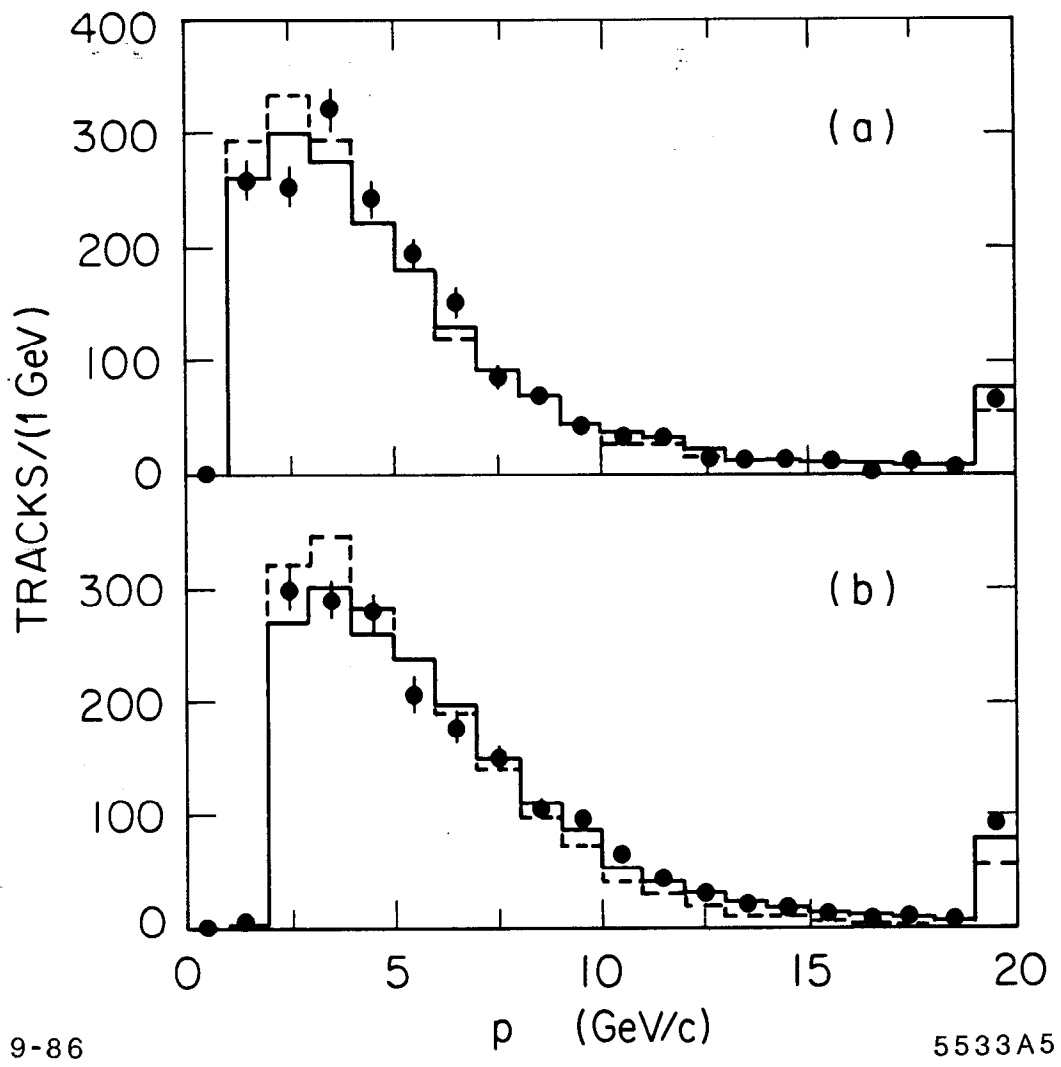


Fig. 4



9-86

5533A5

Fig. 5